Journal of Fluorine Chemistry 245 (2021) 109748

Contents lists available at ScienceDirect

Journal of Fluorine Chemistry

journal homepage: www.elsevier.com/locate/fluor

Phase transition in $RbCdZrF_7$: Structure and thermal properties

Evgeniy V. Bogdanov [a,b,*], Maxim S. Molokeev [a,c], Mikhail V. Gorev [a,c], Andrey V. Kartashev [a], Natalia M. Laptash [d], Igor N. Flerov [a,c]

[a] Kirensky Institute of Physics, Federal Research Center KSC SB RAS, 660036 Krasnoyarsk, Russia
[b] Institute of Engineering Systems and Energy, Krasnoyarsk State Agrarian University, 660049 Krasnoyarsk, Russia
[c] Institute of Engineering Physics and Radioelectronics, Siberian Federal University, 660074 Krasnoyarsk, Russia
[d] Institute of Chemistry, Far Eastern Branch of RAS, 690022 Vladivostok, Russia

ARTICLE INFO

Keywords:
Phase transition
Fluorides
Structure
Heat capacity
Entropy
Thermal expansion

ABSTRACT

X-ray, calorimetric and dilatometric studies of $RbCdZrF_7$ revealed the existence of the second order phase transition $Cmcm \leftrightarrow P2_1/m$ at $T_0 = 200$ K. The structure of the initial and distorted phases is ordered. The phase transition is associated with displacements of fluorine atoms, which leads to minor rotations of the CdF_7 and ZrF_7 pentagonal bipyramids. A small change in entropy, $0.1R$, is characteristic of displacive-type transformations. An anomalously high susceptibility of the transition temperature to hydrostatic pressure was found.

1. Introduction

For a long time, materials based on zirconium and hafnium fluoride complexes have been actively investigated for their potential use. Numerous and comprehensive studies have shown that many of these crystals exhibit important practical properties [1], such as superionic conductivity [2,3], ferroelectricity [4], visible luminescence [5] and X-ray luminescence [6] In addition, zirconium and hafnium fluorides are suitable for optical applications as compact solid-state laser sources at wavelengths from UV to mid-IR [7,8].

Among the large number of zirconium and hafnium heptafluoride complexes, there are several series of crystals, for example $A^+{}_3M^{4+}F_7$ [9–11] and $A^+M^{2+}M^{4+}F_7$ (A^+: K, NH_4, Rb, Tl; M^{2+}: Mn, Cu, Cd, Ca; M^{4+}: Zr, Hf) [12–14], a remarkable feature of which is the presence in the structure of seven-coordinated pentagonal bipyramid $M^{4+}F_7$. Despite the low symmetry of these anionic structural units, the former group of fluoride complexes exhibits cubic symmetry in the initial phase, *Fm*-3*m* ($Z = 4$), which can decrease during structural phase transitions initiated by changes in temperature and/or external hydrostatic, as well as internal chemical pressure. The latter tool plays a significant role in the formation of sequences of structural distortions and corresponding physical properties.

Ammonium heptafluoridozirconate, $(NH_4)_3ZrF_7$, undergoes six structural transformations in a narrow temperature range (240–290) K: *Fm*-3*m* ↔ *F*23 ↔ *Immm* ↔ *I*2/*m* ↔? ↔ *P*-1 ↔ monoclinic [15,16]. Partial and complete replacement of the tetrahedral ammonium cation with spherical potassium, on the one hand, does not change the cubic symmetry of the initial phase, but, on the other hand, leads to a strong decrease in the number of phase transitions and a significant difference in the symmetry of the distorted phases, which are purely individual for each of the compounds: $(NH_4)_2KZrF_7$ - *Fm*-3*m* ↔ $P4_2/ncm$ ↔ $P4_2/nmc$ [17]; K_3ZrF_7 – *Fm*-3*m* ↔ *R*-3*m* [18]. Moreover, the total entropy change associated with the change in symmetry from cubic to the lowest-symmetric also decreases: $(NH_4)_3ZrF_7$ – $\Delta S \approx R\ln 5.7$ [16]; $(NH_4)_2KZrF_7$ – $\Delta S \approx R\ln 2.6$ [19]; K_3ZrF_7 – $\Delta S \approx R\ln 1.4$ [18].

Analysis of the structural models of the initial and distorted phases in combination with the entropy parameters of transitions allowed us to assume that even in $(NH_4)_3ZrF_7$, despite the rather large value of the total experimental entropy, the mechanism of each of the individual structural distortions is not associated with any order-disorder processes, but with a different degree of anharmonicity of fluctuations of critical structural units.

The structure of another group of fluoride complexes, $A^+M^{2+}M^{4+}F_7$, with a seven-coordinated polyhedron $M^{4+}F_7$ can be considered as a derivative of $A^+{}_3M^{4+}F_7$, formed by replacing two monovalent atoms with a divalent one, which is also surrounded by seven fluorine atoms. The symmetry of these compounds was lower than cubic and depended on the ionic radius of the divalent cation (CN = 7): orthorhombic, *Cmcm*

* Corresponding author at: Kirensky Institute of Physics, Federal Research Center KSC SB RAS, 660036Krasnoyarsk, Russia.
E-mail address: evbogdanov@iph.krasn.ru (E.V. Bogdanov).

https://doi.org/10.1016/j.jfluchem.2021.109748
Received 15 December 2020; Received in revised form 8 February 2021; Accepted 11 February 2021
Available online 15 February 2021

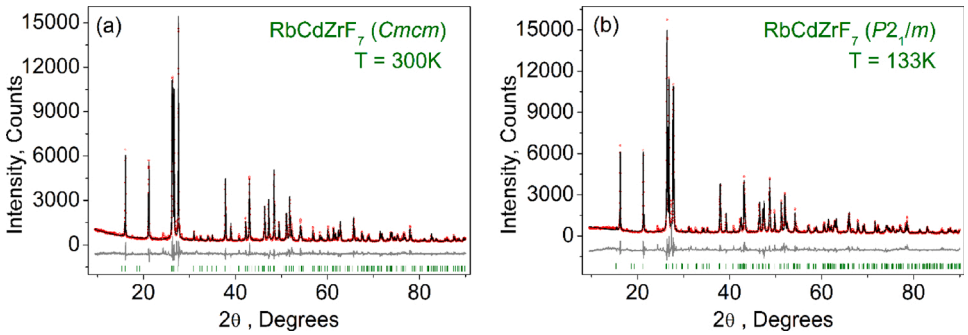

Fig. 1. Difference Rietveld plot of $RbCdZrF_7$ measured at: $T = 300$ K (*a*); $T = 133$ K (*b*).

($Z = 4$), for the case of M^{2+}: Cd (1.03 Å), Ca (1.06 Å) [12] and monoclinic, $P2_1/m$ ($Z = 2$) for M^{2+}: Mn (0.9 Å) [13]. That is, a decrease in the volume of the unit cell due to a change in chemical pressure leads to a decrease in symmetry. Studies of the structure of $A^+M^{2+}M^{4+}F_7$ heptafluoride complexes were performed only at room temperature, and the question of the possible implementation of transitions between the *Cmcm* and $P2_1/m$ phases during temperature changes, and, as a result, changes in the cell volume, remained open.

The present paper is devoted for the first time to the study of the thermal stability of the *Cmcm* structure in $A^+M^{2+}M^{4+}F_7$ fluoride complexes. To this end, a comprehensive study of the structure, heat capacity, and thermal expansion of $RbCdZrF_7$ was performed over a wide temperature range.

2. Experimental

Caution. Hydrofluoric acid is toxic and corrosive! It must be handled with extreme caution and the appropriate protective gear and training [20–22]. Experiments were done in a fume hood.

Our preparation of $RbCdZrF_7$ is less complicated and requires less time than was previously reported [12]. The starting material, $(NH_4)_3ZrF_7$, was prepared by reacting ZrO_2 with concentrated HF (40 wt.%) followed by the addition of an excess of NH_4F. Reagent grade Rb_2CO_3 and $Cd(OH)_2$ (or CdO) were added in stoichiometric quantities according to the reaction: $(NH_4)_3ZrF_7 + 0.5Rb_2CO_3 + Cd(OH)_2 = RbCdZrF_7 + 3NH_3 + 0.5CO_2 + 2.5H_2O$. The mixture of initial components was thoroughly ground using a mortar and pestle, during which the formation of NH_3 was noticed by its distinct smell and green coloring of wet indicator paper. The mixture was placed in a Pt-cup and heated on a hot plate for removing ammonia. The obtained cake was wetted with a 40% HF solution, evaporated to dryness and placed in a muffle for 2–3 h at 600 °C, which resulted in a homogeneous phase of the complex.

All structural studies of the $RbCdZrF_7$ compound obtained were performed by X-ray method using a Bruker D8 ADVANCE powder diffractometer (Cu-Kα radiation), the Anton Paar temperature attachment and linear VANTEC detector. The 2θ range of 9 – 90° was measured with 0.6 mm divergence slit, the step size of 2θ was 0.016°, and the counting time was 1.2 s per step. Profile fitting, crystal structure searching and Rietveld refinements were performed by using TOPAS 4.22 [23].

XRD characterization of $RbCdZrF_7$ at 300 K showed that almost all structural peaks, with the exception of a small number of tiny impurity peaks, are indexed by a *C*-centered orthorhombic unit cell (Fig. 1*a*) with parameters close to those published earlier [12].

The stability of the initial orthorhombic phase to temperature changes was examined by measuring the thermal properties. For this aim samples were prepared in the form of quasi-ceramic tablets with a diameter of 4 – 8 mm and a thickness of about 1 – 4 mm by pressing at ~ 2 GPa.

At the first stage, preliminary calorimetric measurements were performed using a differential scanning microcalorimeter DSM-10 M (DSM)

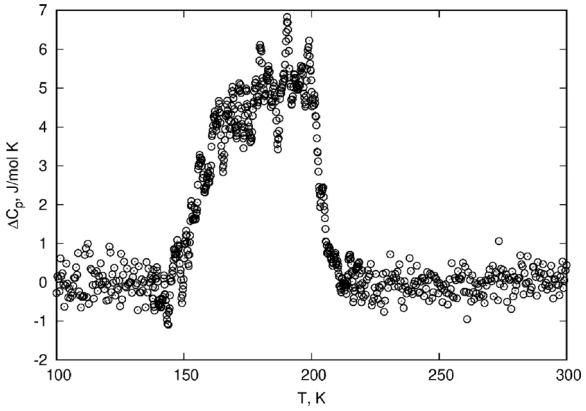

Fig. 2. Anomalous heat capacity, measured by DSM in the heating mode.

in the temperature range of 100 – 400 K in a dry helium atmosphere with a heating rate of 8 K/min on a sample weighing ~ 0.02 g.

Detailed heat capacity studies were carried out in a temperature range of 80 – 315 K by means of a home-made adiabatic calorimeter with three screens [24]. The sample weight was 367.3 mg. In the entire temperature range studied, the error in determining the heat capacity did not exceed (0.4 – 0.8)%. The heat capacity of the "sample + heater + contact grease" system was measured by both discrete and continuous heating. In the first case, the calorimetric step varied from 0.5 to 1.0 K. In the latter case, the system was heated at a rate of $dT/dt \approx 0.02$ K/min. The heat capacity of the heater and contact grease was determined in individual experiments.

Thermal expansion was measured using a push-rod dilatometer

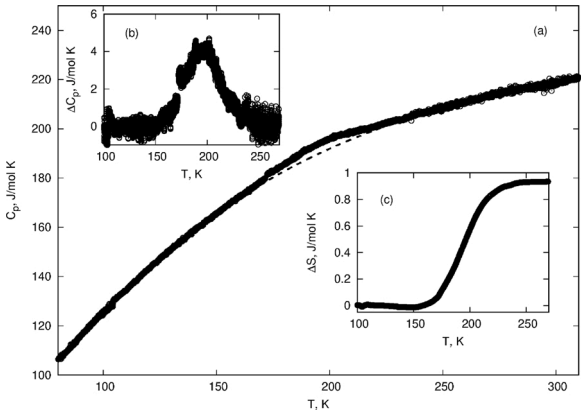

Fig. 3. The temperature dependence of the molar heat capacity (*a*), anomalous heat capacity ΔC_p (*b*) and the excess entropy change (*c*) of $RbCdZrF_7$. Dashed line – lattice specific heat.

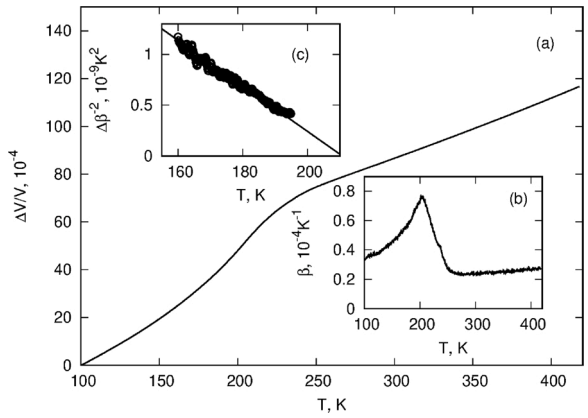

Fig. 4. Temperature dependence of the volume deformation (*a*) and the coefficient of volume thermal expansion (*b*) and $(\Delta\beta)^{-2}$ (*c*) of $RbCdZrF_7$.

(NETZSCH model DIL-402C) with a fused silica sample holder. The experiments were carried out in a dry He flux with a flow rate of ~ 50 mL/min in the temperature range of 100 − 410 K with a heating rate of 3 K/min. To eliminate the influence of thermal expansion of the system, the results were calibrated using quartz as a standard reference. The irreproducibility of the data obtained in successive series of measurements was less than 5%.

3. Results and discussion

In calorimetric experiments using DSM, one small reproducible anomaly was found. Fig. 2 shows the temperature dependence of the excess heat capacity ΔC_p (the difference between the total molar heat capacity C_p and the non-anomalous lattice contribution C_L), which exists in a very wide temperature range, ~ (150 − 205) K. The maximum of ΔC_p was found at temperature $T_0 = 198 \pm 3$ K which was interpreted as the phase transition temperature in heating mode.

Results of the detailed measurements using an adiabatic calorimeter are shown in Fig. 3*a*. Molar heat capacity $C_p = 220$ J/mol K at 310 K is quite close to the limit value $3RN = 250$ J/mol K ($R = 8.314$ J/mol K is the universal gas constant; N is the number of atoms in the formula unit) in accordance with the Neumann–Kopp rule, which allowed us to assume a low characteristic Debye temperature for $RbCdZrF_7$. Analysis of the lattice, C_L, and anomalous, ΔC_p, associated with the phase transition, contributions to the total heat capacity confirmed the validity of our expectations. The procedure for determining the $C_L(T)$ dependence was performed by fitting experimental data on $C_p(T)$ significantly above and below the phase transition region (at $T < 150$ K and at $T > 250$ K) in the framework of the Debye and Einstein models, followed by C_L interpolation over the entire temperature region of the measured heat capacity (Fig. 3*a*). The characteristic Debye and Einstein temperatures were estimated as $\Theta_D = 195$ K and $\Theta_E = 534$ K, respectively

A small and symmetrically blurred peak of the anomalous heat capacity $\Delta C_p(T)$ relative to $T_0 = 197 \pm 2$ K was detected in a very wide temperature range of 150 − 250 K (Fig. 3*b*) Integration of the $\Delta C_p(T)$ function over the entire range of existence of excess heat capacity allowed us to determine the enthalpy change associated with the phase transition as $\Delta H_0 = 225 \pm 20$ J/mol. The corresponding entropy change was $\Delta S_0 = \int(\Delta C_p/T)dT = 1.0 \pm 0.2$ J/mol K (Fig. 3*c*). Such a small entropy allows us to confidently assume that structural distortions in $RbCdZrF_7$ cannot be associated with any order-disorder processes during the phase transition.

Fig. 4 shows the results of a study of the thermal expansion of $RbCdZrF_7$. The volume strain, $\Delta V/V_0 = 3\cdot(\Delta L/L_0)$, increases monotonically with increasing temperature over the entire range of 100 − 410 K, but its total change is very small, ~ 1%. A smooth inflection on the dependence $\Delta V/V_0(T)$ (Fig. 4*a*) is observed in approximately the same region where the anomalous behavior of the heat capacity is detected (Fig. 3*b*). More clearly, the anomalous behavior of thermal expansion associated with the phase transition can be seen in the dependence of the volume expansion coefficient $\beta = 3\alpha$ (Fig. 4*b*), whose behavior is characterized by a significant difference in comparison with the heat capacity. The β anomaly is a sharp peak with a maximum at $T_0 \approx 200$ K instead of a blurred bump ΔC_p. Such a strong difference in the behavior of two related thermal properties can be explained by the fact that although they are studied on ceramic samples of the same type, linear deformation $\Delta L/L_0$ is measured along one direction, which can be characterized by a significant texture, while $C_p(T)$ is a volume property.

The behavior of C_p and β is typical for second-order phase transition. The presence of a pronounced nonlinear temperature dependence $\beta(T)$ below T_0 allows us to analyze the degree of proximity of the transition to the tricritical point. According to the phenomenological theory of phase transitions, the inverse square of Δβ is a linear function of temperature [25]. Fig. 4*c* shows that this condition is satisfied in a fairly wide range and a significant value of $N = [(T_{tcp}\text{-}T_0)/T_0]^{1/2} \approx 0.3$ indicates that the phase transition in $RbCdZrF_7$ is very far from the tricritical point $T_{tcp} \approx$ 213.5 K at which $N = 0$ and $C_p \rightarrow \infty$.

The strong blurring of the heat capacity anomaly also prevented direct measurements of the effect of external pressure on the phase transition temperature in $RbCdZrF_7$ using the highly sensitive method that we successfully used earlier for constructing temperature-pressure phase diagrams of a large number of fluoride complexes and oxyfluorides [26]. Estimation of the volume baric coefficient using the Ehrenfest equation $dT/dp = T_0\cdot V_m\cdot\Delta\beta/\Delta C \approx 220$ K/GPa (here V_m is the molar volume) indicates a very high sensitivity of $RbCdZrF_7$ to hydrostatic pressure.

Table 1
Main parameters of processing and refinement of the sample $RbCdZrF_7$.

T, K	300	133
Sp.Gr.	*Cmcm*	$P2_1/m$
a, Å	6.7796 (1)	6.4486 (2)
b, Å	11.0672 (2)	8.4042 (2)
c, Å	8.4240 (2)	6.4745 (2)
β, °	–	116.794 (1)
V, Å^3	632.06 (2)	313.22 (2)
Z	4	2
2θ-interval, °	9−90	9−90
R_{wp}, %	10.07	13.07
R_p, %	7.43	9.54
R_{exp}, %	4.19	4.24
χ^2	2.40	3.08
R_B, %	3.55	4.41

Table 2
Fractional atomic coordinates and isotropic displacement parameters (Å^2).

Atom	x	y	z	B_{iso}
$T = 300$ K				
Rb	0.5	0	0	2.7 (4)
Cd	0	0.1897 (4)	0.25	1.3 (4)
Zr	0.5	0.3074 (4)	0.25	0.7 (4)
F1	0.5	0.4650 (15)	0.25	2.7 (4)
F2	0.322 (3)	0.1527 (12)	0.25	2.7 (4)
F3	0.225 (3)	0.3600 (14)	0.25	2.7 (4)
F4	0.5	0.2991 (9)	0.003 (5)	2.7 (4)
$T = 133$ K				
Rb	0.5	0	0.5	1.0 (3)
Cd	0.1938 (9)	0.25	0.8138 (10)	0.5 (4)
Zr	0.8120 (11)	0.25	0.1976 (13)	0.5 (4)
F1	0.928 (4)	0.25	0.008 (5)	1.1 (4)
F2	0.492 (4)	0.25	0.193 (5)	1.1 (4)
F3	0.898 (4)	0.25	0.588 (6)	1.1 (4)
F4	0.596 (4)	0.25	0.881 (5)	1.1 (4)
F5	0.151 (5)	0.25	0.423 (6)	1.1 (4)
F6	0.755 (2)	0.007 (3)	0.147 (3)	1.1 (4)

Table 3
Main bond lengths (Å).

T = 300 K			
Rb—F2	2.957 (10)	Cd—F4^{i}	2.13 (5)
Rb—F3^{i}	3.028 (12)	Zr—F1	1.745 (17)
Cd—F1^{ii}	2.487 (17)	Zr—F2	2.093 (15)
Cd—F2	2.224 (17)	Zr—F3	1.951 (18)
Cd—F3	2.426 (17)	Zr—F4	2.08 (5)
T = 133 K			
Rb—F2	2.876 (18)	Cd—F6^{iv}	2.18 (3)
Rb—F4	3.08 (2)	Zr—F1	1.701 (19)
Rb—F5	2.951 (11)	Zr—F2	2.050 (14)
Cd—F1^{i}	2.542 (15)	Zr—F3	2.33 (3)
Cd—F2^{ii}	2.34 (3)	Zr—F4^{v}	1.89 (3)
Cd—F3^{iii}	1.81 (3)	Zr—F5^{vi}	2.01 (2)
Cd—F4	2.428 (13)	Zr—F6	2.08 (3)
Cd—F5	2.42 (3)		

Symmetry codes for the phase at 300 K: (i) -x+1/2, -y+1/2, -z; (ii) -x+1/2, y-1/2, -z+1/2.
Symmetry codes for the phase at 133 K: (i) x, y, z+1; (ii) x-1, y, z; (iii) -x+1, -y, -z+1; (iv) x+1, y, z; (v) x, y, z-1.

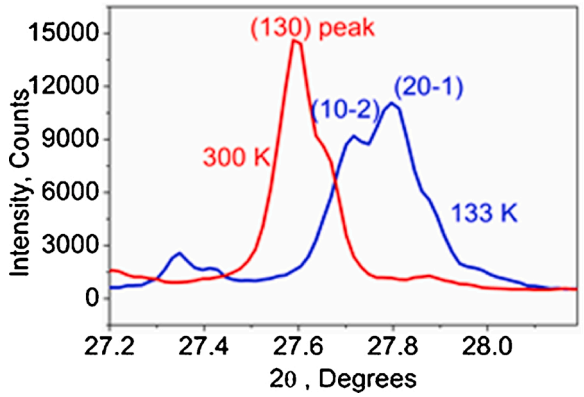

Fig. 5. The (130) peak splitting into (10-2) and (20-1) under cooling from 300 K to 133 K.

Table 4
All possible monoclinic unit cells with k = (0, 0, 0) obtained from *Cmcm*.

Irrep	Space group	Basis
Γ_2^+	$P2_1/m$	(1/2,1/2,0),(0,0,1),(1/2,-1/2,0)
Γ_3^+	$C2/m$	(0,1,0),(1,0,0),(0,0,-1)
Γ_4^+	$C2/c$	(1,0,0),(0,1,0),(0,0,1)

As mentioned above, almost all X-ray peaks of the $RbCdZrF_7$ compound were indexed at 300 K by a *C*-centered orthorhombic unit cell with parameters close to those previously published [12]. Therefore, this structure was taken as the initial model for the Rietveld refinement which was stable and gave low *R*-factors (Table 1, Fig. 1*a*). The coordinates of the atoms and the lengths of the main bonds are presented in Tables 2 and 3, respectively.

When cooling to 133 K, splitting of the main peaks was observed (Figs. 1*b* and 5). The superstructure peaks were not detected (Fig. 1*b*), so it was suggested that the phase transition is associated with cell distortion without multiple increasing the cell volume. In other words, the transformation can be described by the appearance of instability at (0, 0, 0) *k*14 - point (G) of the Brillouin zone of a highly symmetric unit cell *Cmcm* (hereinafter, the notation of irreducible representations (irrep) and points of the Brillouin zone are given in accordance with reference books [27,28]).

Since the main peak is split, therefore, the symmetry of the new phase must be monoclinic or triclinic, but not orthorhombic. It is highly desirable to determine as symmetric a space group as possible for the distorted phase, so monoclinic symmetry was chosen for the first consideration. A list of all possible monoclinic phases with k = (0,0,0) (Table 4) was obtained using the ISODISTORT program [29].

The crystallographic data are deposited in Cambridge Crystallographic Data Centre (CSD # 2050059-2050060). The data can be downloaded from the site (www.ccdc.cam.ac.uk/data_request/cif).

Preliminary fitting of all the proposed cells showed that only one variant of the unit cell with $P2_1/m$ splits the peaks properly and fits well powder pattern at 133 K. The coordinates of the atoms of the $P2_1/m$ crystal structure were calculated by ISODISTORT and used later in the Rietveld refinement. An excellent fit of all intensities and low *R*-factors were obtained (Table 1, Fig. 1*b*). The coordinates of the atoms and the lengths of the main bonds are shown in Tables 2 and 3, respectively. Structural analysis of this distorted phase using the Plato program [30] did not reveal any problems with symmetry, bond lengths, or interstices in the structure, so we can assume that the space group $P2_1/m$ was chosen correctly.

Thus, the $RbCdZrF_7$ crystal undergoes a single phase transition at $T_0 \approx 200$ K, which is associated with small displacements of the structural elements. According to group-theoretic analysis, the Γ_2^+ irrep drives this phase transition. The transformation can be written as $Cmcm \leftrightarrow (\Gamma_2^+(\eta)) \leftrightarrow P2_1/m$ (Fig. 6), where η is the critical order parameter. It should be noted that this irrep allows the phase transition to be continuous, which is consistent with the data from the study of thermal properties. The phase transition leads to a redistribution of the charge order of the F ions with the appearance of a new translation and splitting of positions. For example, both sections F2 and F3 in the *Cmcm* structure (Fig. 6*a*) are divided into two sections in the $P2_1/m$ phase (Fig. 6*b*): F2, F3 and F4, F5, respectively. The ions F1, F2, and F3 of the *Cmcm* phase experience the greatest displacement during the phase transition, and the corresponding shifts are 0.22, 0.14, and 0.44 Å in the *ab* plane (or the *ac* plane of the $P2_1/m$ phase), respectively. These maximum shifts are really not very large and lead only to a small rotation of the pentagonal bipyramids ZrF_7, CdF_7 along the *c* axis of the *Cmcm* phase (or the *b* axis of the $P2_1/m$

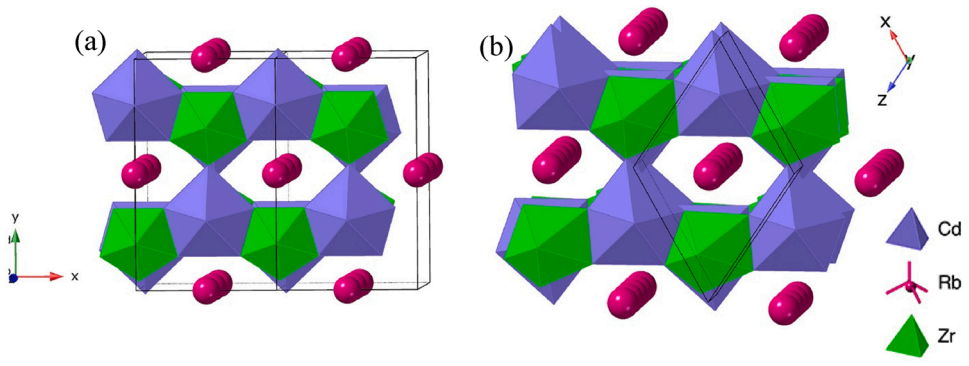

Fig. 6. Crystal structure of $RbCdZrF_7$ at T = 300 K (*a*) and T = 133 K (*b*).

phase) and/or their deformation.

4. Conclusions

For the first time, an investigation of the thermal stability of the *Cmcm* structure in $A^{+}M^{2+}M^{4+}F_7$ fluoride complexes was carried out.

A comprehensive study using calorimetric, dilatometric, and structural methods revealed the existence of a phase transition in $RbCdZrF_7$ at $T_0 = 200$ K. The initial *Cmcm* phase is characterized by relatively small isotropic displacement parameters for all atoms, including fluorines (Table 2), and, as a consequence, is ordered. Structural distortions during the *Cmcm* ↔ $P2_1/m$ phase transition, which lead to an even stronger decrease in B_{iso}, are associated with the rotation of the pentagonal bipyramids CdF_7 and ZrF_7 by a very small angle. This is why the experimentally determined entropy change was very small, $\Delta S_0 \approx 0.1R$, and characteristic of displacive transformations.

In accordance with irrep ($\Gamma 2+(\eta)$), the phase transition under consideration can be continuous which agrees with the behavior of the thermal properties characteristic for the transformations of the second order rather far from the tricritical point.

A remarkable feature is that $RbCdZrF_7$ demonstrates very high sensitivity to external pressure with the baric coefficient $dT_0/dp = 220$ K/GPa which can be useful at design of effective materials based on $A^{+}M^{2+}M^{4+}F_7$ heptafluoride complexes.

It seems very interesting to continue studies on crystals with an ammonium group, for example, NH_4MnZrF_7 [13], demonstrating the monoclinic symmetry $P2_1/m$ at room temperature.

Declaration of Competing Interest

The authors declare that they have no known competing financial interests or personal relationships that could have appeared to influence the work reported in this paper.

Acknowledgements

The reported study was funded by RFBR according to the research project No. 18-02-00269 a. X-ray and dilatometric data were obtained using the equipment of Krasnoyarsk Regional Center of Research Equipment of Federal Research Center "Krasnoyarsk Science Center SB RAS".

References

[1] A. Tressaud (Ed.), Functionalized Inorganic Fluorides: Synthesis, Characterization and Properties of Nanostructured Solids, Wiley-Blackwell, 2010, https://doi.org/10.1002/9780470660768.

[2] K.J. Mallikarjunaiah, K.P. Ramesh, R. Damle, ^{1}H and ^{19}F NMR relaxation time studies in $(NH_4)_2ZrF_6$ superionic conductor, Appl. Magn. Reson. 35 (2009) 449–458, https://doi.org/10.1007/s00723-009-0176-2.

[3] V.Ya. Kavun, N.F. Uvarov, A.B. Slobodyuk, V.K. Goncharuk, A.Yu. Kotenkov, I. A. Tkachenko, A.V. Gerasimenko, V.I. Sergienko, Ionic mobility, phase transitions, and superionic conduction in solid solutions (100-x)PbF_2–xZrF_4 and crystals K_2ZrF_6, $(NH_4)_2ZrF_6$, $KSnZrF_7$, and m$(NH_4)_6Zr_4F_{23}$ (M = Li, Na), Russ. J. Electrochem. 41 (2005) 501–509, https://doi.org/10.1007/s11175-005-0096-x.

[4] M.R. Bauer, D.L. Pugmire, B.L. Paulsen, R.J. Christie, D.J. Arbogast, C.S. Gallagher, W.V. Raveane, R.M. Nielson, C.R. Ross II, P. Photinos, S.C. Abrahams, Aminoguanidinium hexafluorozirconate: a new ferroelectric, J. Appl. Crystallogr. 34 (2001) 47–54, https://doi.org/10.1107/S0021889800015508.

[5] C.C. Underwood, C.D. McMillen, H. Chen, J.N. Anker, J.W. Kolis, Hydrothermal Chemistry, Structures, and Luminescence Studies of Alkali Hafnium Fluorides, Inorg. Chem. 52 (2013) 237–244, https://doi.org/10.1021/ic301760a.

[6] M.M. Godneva, N.N. Boroznovskaya, D.L. Motov, V.M. Klimkin, N.L. Mikhailova, Thermal stability and X-ray-luminescent properties of fluorozirconates and fluorosulfatozirconates, Russ. J. Inorg. Chem. 54 (2009) 563–567, https://doi.org/10.1134/S0036023609040123.

[7] V. Nazabal, M. Poulain, M. Olivier, P. Pirasteh, P. Camy, J.-L. Doualan, S. Guy, T. Djouama, A. Boutarfaia, J.L. Adam, Fluoride and oxyfluoride glasses for optical applications, J. Fluorine Chem. 134 (2012) 18–23, https://doi.org/10.1016/j.jfluchem.2011.06.035.

[8] J.-L. Adam, Non-oxide glasses and their applications in optics, J. Non-Cryst. Solids 287 (2001) 401–404, https://doi.org/10.1016/S0022-3093(01)00632-9.

[9] A. Rakhmatullin, M. Boča, J. Mlynáriková, E. Hadzimová, Z. Vasková, I.B. Polovov, M. Mičušík, Solid state NMR and XPS of ternary fluorido-zirconates of various coordination modes, J. Fluorine Chem. 208 (2018) 24–35, https://doi.org/10.1016/j.jfluchem.2018.01.010.

[10] M.T. Dova, M.C. Caracoche, A.M. Rodriguez, J.A. Martinez, P.C. Rivas, A.R. Lopez Garcia, Time-differential perturbed-angular-correlation study of phase transitions and molecular motions in K_3(Hf,Zr)F_7, Phys. Rev. B40 (1989) 11258–11263, https://doi.org/10.1103/PhysRevB.40.11258.

[11] R.L. Davidovich, D.V. Marinin, V. Stavila, K.H. Whitmire, Stereochemistry of fluoride and mixed-ligand fluoride complexes of zirconium and hafnium, Coord. Chem. Rev. 257 (2013) 3074–3088, https://doi.org/10.1016/j.ccr.2013.06.016.

[12] L. Meddar, M. El-Ghozzi, D. Avignant, New Heptafluorozirconates and -hafnates $A^{I}B^{II}Zr(Hf)F_7$ (A^{I} = Rb, Tl; B^{II} = Ca, Cd) – Synthesis, Structures, and Structural Relationships, Z. Anorg. Allg. Chem. 634 (2008) 565–570, https://doi.org/10.1002/zaac.200700465.

[13] M. El-Ghozzi, D. Avignant, M. Guillot, Synthesis, structures, and characterization of $MMnZrF_7$ (M=Tl, Rb, NH_4, K) fluorides: an example of 7-Coordination of divalent manganese, J. Solid State Chem. 108 (1994) 51–58, https://doi.org/10.1006/jssc.1994.1008.

[14] M. Kraus, B.G. Müller, $KCuM^{IV}F_7$ (M^{IV} = Zr^{4+}, Hf^{4+}), ein neuer Strukturtyp, Z. Anorg. Allg. Chem. 626 (2000) 1929–1933, https://doi.org/10.1002/1521-3749(200009)626:9<1929::AID-ZAAC1929>3.0.CO;2-P.

[15] S.V. Misyul, S.V. Mel'nikova, A.F. Bovina, N.M. Laptash, Optical and x-ray diffraction studies of the symmetry of distorted phases of the $(NH_4)_3ZrF_7$ crystal, Phys. Solid State 50 (2008) 1951–1956, https://doi.org/10.1134/S1063783408100272.

[16] V. Fokina, M. Gorev, E. Bogdanov, E. Pogoreltsev, I. Flerov, N. Laptash, Thermal properties and phase transitions in $(NH_4)_3ZrF_7$, J. Fluorine Chem. 154 (2013) 1–6, https://doi.org/10.1016/j.jfluchem.2013.07.001.

[17] E. Pogoreltsev, S. Melnikova, M. Molokeev, I. Flerov, N. Laptash, Structural, thermal and optical properties of elpasolite-like $(NH_4)_2KZrF_7$, J. Solid State Chem. 277 (2019) 376–380, https://doi.org/10.1016/j.jssc.2019.06.013.

[18] M.V. Gorev, M.S. Molokeev, A.V. Kartashev, E.I. Pogoreltsev, S.V. Mel'nikova, N. M. Laptash, I.N. Flerov, Investigation of thermal properties and structure of complex fluoride K_3ZrF_7, J. Fluorine Chem. 241 (2021) 109677, https://doi.org/10.1016/j.jfluchem.2020.109677.

[19] M.V. Gorev, A.V. Kartashev, E.V. Bogdanov, I.N. Flerov, N.M. Laptash, Calorimetric, dilatometric and DTA under pressure studies of the phase transitions in elpasolite $(NH_4)_2KZrF_7$, J. Fluorine Chem. 235 (2020) 109523, https://doi.org/10.1016/j.jfluchem.2020.109523.

[20] J.C. Bertolini, Hydrofluoric acid: a review of toxicity, J. Emerg. Med. 10 (1991) 163–168, https://doi.org/10.1016/0736-4679(92)90211-B.

[21] D. Peters, R. Miethchen, Symptoms and treatment of hydrogen fluoride injuries, J. Fluorine Chem. 79 (1996) 161–165, https://doi.org/10.1016/S0022-1139(96)03484-7.

[22] E.B. Segal, First aid for a unique acid, HF: a sequel, Chem. Health Saf. 7 (2000) 18–23, https://doi.org/10.1021/acs.chas.8b07106.

[23] A.X.S. Bruker, TOPAS V4: General Profile and Structure Analysis Software for Powder Diffraction Data. – User's Manual, Bruker AXS, Karlsruhe, Germany, 2008.

[24] A.V. Kartashev, I.N. Flerov, N.V. Volkov, K.A. Sablina, Adiabatic calorimetric study of the intense magnetocaloric effect and the heat capacity of $(La_{0.4}Eu_{0.6})_{0.7}Pb_{0.3}MnO_3$, Phys. Solid State 50 (2008) 2115–2120, https://doi.org/10.1134/S1063783408110188.

[25] I.N. Flerov, M.V. Gorev, I.M. Iskornev, Calorimetric and dilatometric study of the ferroelastic phase transitions in the elpasolites, Ferroelectrics 48 (1983) 97–102, https://doi.org/10.1080/00150198308227844.

[26] M.V. Gorev, E.V. Bogdanov, I.N. Flerov, T-p phase diagrams and the barocaloric effect in materials with successive phase transitions, J. Phys. D Appl. Phys. 50 (2017) 384002, https://doi.org/10.1088/1361-6463/aa8025.

[27] O.V. Kovalev, Representations of the Crystallographic Space Groups: Irreducible Representations, Induced Representations, and Corepresentations, Gordon and Breach Science, 1993.

[28] S.C. Miller, W.F. Love, Tables of Irreducible Representations of Space Groups and Co-representations of Magnetic Space Groups, Pruett Press, 1967.

[29] B.J. Campbell, H.T. Stokes, D.E. Tanner, D.M. Hatch, ISODISPLACE: a web-based tool for exploring structural distortions, J. Appl. Crystallogr. 39 (2006) 607–614, https://doi.org/10.1107/S0021889806014075.

[30] A.L. Speck, Validation of a single-crystal structure using the Plato program, J. Appl. Crystallogr. 36 (2003) 7–13, https://doi.org/10.1107/S0021889802022112.